International Journal of
INTELLIGENT SYSTEMS AND APPLICATIONS IN ENGINEERING
ISSN:2147-6799 www.ijisae.org Original Research Paper

A Novel CNN Framework for the Detection of COVID-19 Using Manta Ray Optimization and KNN Classifier in LUS Images

Gayathri J L[1], Bejoy Abraham*[2], Sujarani M S[3], Sivakumar Ramachandran[4]

Submitted: 15/11/2022 **Accepted:** 16/02/2023

Abstract: Reverse transcription polymerase chain reaction (RT-PCR) is the gold standard for the diagnosis of COVID-19. Studies have proven that non-invasive techniques based on medical imaging can be used as an alternative to RT-PCR. The use of medical imag- ing technologies along with RT-PCR could improve the diagnosis and management of the disease. Even though several methods exist for diagnosing COVID-19 from X- ray images and CT scans, ultrasound image has not been explored much to diagnose the disease. In this study, we built a deep learning model using ultrasound images for a fast and efficient disease diagnosis. Pre-trained Convolutional Neural Networks (CNN), trained on the ImageNet database has been utilized for feature extraction. The nature-inspired Manta Ray Foraging Optimization (MRFO) algorithm is applied for dimensionality reduction and K-Nearest-Neighbour (KNN) for classification. Model training has been performed using a publicly available POCUS dataset consisting of 2944 ultrasound images sampled from more than 200 Lung Ultrasound (LUS) videos. Experimentations conducted in this study prove the efficiency of the model in the diagnosis of COVID-19. The model achieved an accuracy of 99.4337% using MobilenetV2 as the pre-trained network.

Keywords: *CNN, COVID-19, K-Nearest-Neighbour, Manta Ray Foraging Optimization.*

1. Introduction

Millions of lives have been inflicted due to several infectious diseases in the past decades. On December 31, 2019, Wuhan City became a cynosure of unidentified pneumonia, which has shaken the world quickly. On January 7, 2020, the cause of pneumonia was identified and momentarily named as 2019-nCoV [1]. The disease has been engendered by a newly discovered virus called Severe Acute Respiratory Syndrome Coronavirus 2 (SARS-CoV-2). Coronavirus belongs to a large family of viruses that could inflict diseases ranging from asymptotic symptoms to severe illness [2]. The disease can cause serious illness to people with underlying medical conditions and even lead to death. The death toll due to the pandemic has risen more than 53 lakhs up to the end of December 2021. The period of transmission of the virus since the appearance of symptoms is estimated to be within a week [3]. The death toll caused by the corona virus is greater than other influenza viruses. Mild symptoms include cough, fever, and headache, whereas severe symptoms are accompanied by shortness of breath, affecting the lungs. The virus transmission occurs through tiny droplets from the mouth or nose, which are spread when a person with COVID-19 coughs or exhales.

Circulation of the virus among the population has increased the chances of virus mutations. Genetic variants of the virus increased the spread to a great extent [7]. RT- PCR test is widely accepted as the standard for confirmation of the disease. Resource and time constraints made early detection of the disease a big challenge. Clinical findings have proven that images obtained from Computed Tomography (CT), X-rays, and, Ultrasound (US) modalities exhibit abnormal lung findings on infected patients. Chest X-rays exhibits multifocal, bilateral ground-glass opacity patterns and consolidations with peripheral and basal predominance in COVID-19 patients [8]. Ground glass opacities, vascular expansion, bilateral abnormalities, lower lobe involvement, and posterior predilection are the CT image findings observed in the cases of COVID-19 [9]. Radiological observations in ultrasound images are pulmonary consolidation, thickened pleural lines, and a small amount of pleural effusions observed on some patients [10]. Rapid spread of the virus has led manual examination of the radiographic im- ages, a cumbersome task for the medical professionals. Hence, there is a need for Computer-Aided-Detection (CAD) techniques, which can assist radiologists in quickly diagnosing the disease. In this work, images

[1] *Department of Computer Science and Engineering, College of Engineering Perumon, Kollam, Kerala, India*
ORCID ID : 0000-0001-7491-425X
[2] *Department of Computer Science and Engineering, College of Engineering Muttathara, Thiruvananthapuram, Kerala, India*
ORCID ID : 0000-0002-5920-8629
[3] *Department of Computer Science and Engineering, College of Engineering Perumon, Kollam, Kerala, India*
ORCID ID : 0000-0003-1809-4570
[4] *Department of Electronics and Communication Engineering, College of Engineering Trivandrum, Kerala, India*
ORCID ID : 0000-0002-1621-5490
** Corresponding Author Email: bjoyabraham@gmail.com*

obtained from ultrasound diagnostic technique has been utilized for the construction of the proposed model. Compared to other image modalities, lung ultrasound shows more sensitivity in diagnosing the disease. Ultrasound images can be obtained bedside without the patient being exposed to harmful radiations. When lesion locations are adjacent to the pleura, lung ultrasounds are more likely to detect the lesions earlier than the chest radiographs. Usage of the Point-of-Care-Ultrasound (POCUS) technique reduces the exposure of the virus to the technicians and medical staff attending the case, which mitigates the spread of the virus.

The literature provides substantial research works that use images obtained from CT and chest X-ray modalities for COVID-19 detection [11, 12, 13, 14, 15]. However, the techniques employing ultrasound images for disease prediction is very less. Born et al. [4] adopted transfer learning methodology for computer-aided diagnosis of COVID-19. POCUS dataset consisting of 64 video recordings were utilized for the model training. The model utilized pre-trained VGG-16 network as the backbone augmented with an additional five convolution layers. The model was trained for COVID- 19, Pneumonia and healthy classes. Muhammad and Hossain [16] constructed a CNN framework employing multi-layer fusion functionality to improve the screening efficiency of COVID-19. Experimental evaluation of the model was conducted using publicly available lung ultrasound images and video samples. Awasthi et al. [17] developed a MobileNet based light weight network named as Mini-COVIDNet that involves fine-tuning of MobileNet network, which is light in size utilizing US dataset. The work by Bagon et al. [18] involves fine-tuning of the image classification model for the diagnosis of COVID-19 using lung ultrasound images. The model utilized ICLUS dataset consisting of 277 videos of 35 patients. The above-mentioned works explored end-to-end networks for the diagnosis of COVID-19. The proposed study is one among a few works to distinguish between COVID-19, pneumonia and healthy patients from ultrasound images.

The following are the contributions of the proposed work:

1. The method employs a novel pipeline consisting of pre-trained convolutional neural networks, Manta ray Foraging Optimization Algorithm and K-Nearest Neighbour (KNN) classifier.
2. To the extent of our knowledge no works have explored the combination of pre- trained CNN with an off-the shelf classifier for detecting the disease in lung ultrasound images.
3. Performance evaluation of the proposed method has been conducted empirically using various pre-trained CNNs, feature selection techniques and classifiers.
4. The results obtained using the proposed pipeline outperform that of the state-of- the-art techniques present in the literature.

2. Materials and Methods

2.1. Dataset

The proposed method utilizes Point-Of-Care Ultrasound (POCUS) dataset [4, 5, 6] to evaluate the performance of the designed pipeline. The dataset is being updated regularly. At the time of performing experiments reported in this work, the dataset consists of more than 200 LUS videos and 59 images captured from convex and linear probes. Only convex videos in the dataset have been utilised in the proposed model. For the image dataset creation, the LUS videos and images were merged. The images were extracted from the videos, at a frame rate of 3 Hz with a maximal range of 30 frames per video. The resulting dataset contain 969 COVID-19, 714 Pneumonic and 1261 healthy ultrasound images [4] for evaluating the performance of the proposed pipeline. Figure 1 displays sample images from the dataset belonging to various categories

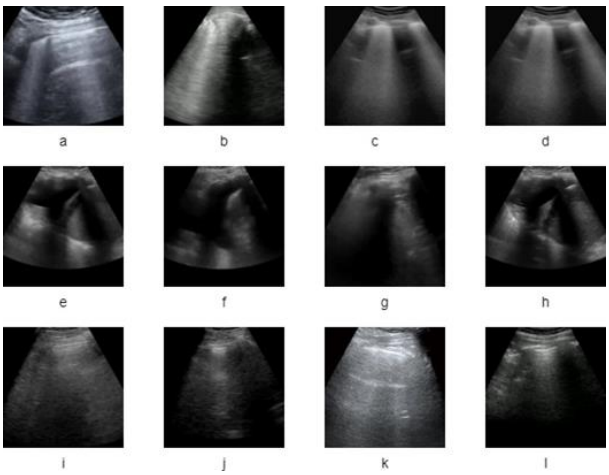

Fig. 1. Sample lung ultrasound images obtained from POCUS dataset [4, 5, 6]. The first, second and third row represent COVID-19, Pneumonia and normal images, respectively

2.2. Methodology

The proposed method employs three main stages, namely a feature extraction stage, a feature selection unit, and a classification phase that maps the feature set to the predictor variables. Figure 2 demonstrates the architecture of the proposed pipeline. The detailed description of the three stages is elaborated in the following sections.

2.2.1. Feature Extraction

The feature extraction process aims to represent the raw data to a more manageable set for further processing. Feature extraction from lung ultrasound images enables the

identification of nonlinearities, thereby identifying the abnormalities present in the lungs. Handcrafted feature extraction techniques commonly used to detect COVID-19 from lung CT or X-ray images include discrete wavelet transform, Haralick texture features, and gray-level co-occurrence matrix. In addition, to characterize textural information, the features are extracted using the fractional multichannel exponent moments, residual exemplar local binary pattern, two-dimensional curvelet transform, histogram of oriented gradients, dual-tree complex contourlet transform, local binary pattern, and multichannel fractional-order Legendre Fourier moments. Similarly, a substantial amount of research used CNN models to detect COVID-19 from lung CT or X-ray im- ages. The CNN models employing the architectures such as DenseNet-201, AlexNet, VGG19, VGG16, Inceptionv3, ResNet101, SqueezeNet, Xception, MobileNetv2 and GoogLeNet have been extensively used for feature learning and extraction to detect COVID-19 in lung CT or X-ray images.

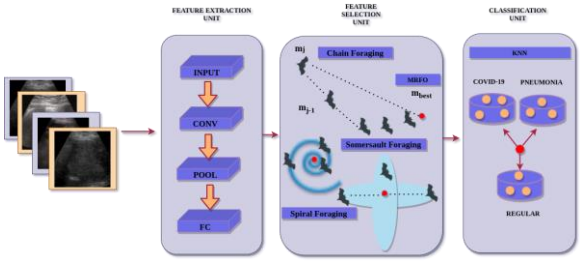

Fig. 2. Architecture of proposed framework

Instead of designing an end-to-end architecture in the proposed CNN framework, we used CNN for feature extraction alone. Pre-trained networks trained on the Imagenet dataset [19], is used as the feature extractor. The 11 pretrained neural networks were trained on Imagenet dataset [19] that consist of more than a million images to categorize images into 1000 classes. These pre-trained networks differ in the number of convolutional layers, input sizes and layer depth. The images are pre-processed to the dimension of the input layer corresponding to the pre-trained network. From the large number of images present in Imagenet dataset, the individual network has learned rich feature representations.

From each of the LUS training images 1000 features are extracted from the last fully connected layers of the pre-trained networks. The output of the feature extraction unit is 2D matrix of dimension n x 1000, where n is the number images supplied into the network.

2.2.2. Feature Selection

In the proposed model, a feature selection module has been integrated to designate the best features for the prediction variables in hand. The model uses MRFO algorithm [20] inspired by the foraging behaviours of Manta rays, the marine creatures. These creatures have large, flat, diamond-formed bodies, which are distinguished by their triangular pectoral fins, and use innovative techniques while feeding. They nourish on plankton, the marine drifters that float along with the tides and the ocean currents. The algorithm mimics the marine creatures three foraging behaviours-chain foraging, cyclone foraging, and somersault foraging.

2.2.3. Chain Foraging

Manta Rays are known to feed in clusters exhibiting cooperative behaviour. They stack up themselves in long chains with each ray swimming above the one ahead. This behaviour is presumed to catch maximum plankton, which would have been escaped from the way of individual swimming. Consequently, they could feed on a large number of plankton with this cooperative behaviour. This chain foraging behaviour is utilized in MRFO [20]. In MRFO, manta rays can make observations on the position of plankton and swim towards it. Higher the number of plankton in a position, better is the position. Nevertheless, the best position is not known, the position with highest quantity of plankton, so far discovered is assumed to be the best solution. Manta rays stack up in line constructing a chain. Each of the manta rays follow the planktons as well as the one moving ahead of it except the rays at the head. Chain foraging can be mathematically represented as:

$$m_j^d(t+1) = \begin{cases} m_j^d(t) + v.(m_{best}^d(t)) + \\ \delta.(m_{best}^d(t) - m_j^d(t)), j = 1 \\ m_j^d(t) + v.(m_{j-1}^d(t) - m_j^d(t)) + \\ \delta.(m_{best}^d(t) - m_j^d(t)), j = 2, \ldots, N \end{cases} \quad (1)$$

$$\delta = 2.v\sqrt{|logv|} \quad (2)$$

where $m_j^d(t)$ represents the position of j^{th} sample in d^{th} dimension at time t, v is a vector whose values lie in the range of [0,1], δ denotes the corresponding weight coefficient [20]. Each individuals updates the position by, the best position ahead of it at each iteration, thereby finding the best solution.

2.2.4. Cyclone Foraging

Manta ray discovers plankton blotches in ocean waters and assembles spirally towards the nourishment constructing a long chain. In cyclone foraging strategy, more than following the food spirally, manta rays follow the individuals ahead [20]. The cyclone foraging of manta rays can be mathematically represented as:

$$m_j^d(t+1) = \begin{cases} m_{best}^d(t) + v.(m_{best}^d(t) - m_j^d(t)) + \\ \rho.(m_{best}^d(t) - m_j^d(t)), j = 1 \\ m_{best}^d(t) + v.(m_{j-1}^d(t) - m_j^d(t)) + \\ \rho.(m_{best}^d(t) - m_j^d(t)), j = 2, \ldots, N \end{cases} \quad (3)$$

$$\rho = 2e^{v_1 \frac{T-t+1}{T}} . sin(2\pi v_1) \quad (4)$$

where δ depicts the weight constant, v_1 represents a random vector in the range of [0,1] and T denotes the maximum number of iterations [20].

2.2.5. Somersault Foraging

In somersault foraging, each individual initially fixes a location of nourishment as the pivot. After that, each manta ray swims back and forth from one location to another in the search space around the pivot and then take a somersault to another position [20]. The mathematical model for somersault foraging can be depicted as:

$$m_j^d(t+1) = m_j^d(t) + s.\left(v_2.m_{best}^d - v_3.m_j^d(t)\right), j = 1,..,N \quad (5)$$

where *s* is the somersault factor, v_2 and v_3 are random vectors that falls in the range of [0,1].

2.2.6. Classification

In the classification phase of the model, the KNN classifier is utilized. KNN is a supervised learning classifier for solving classification and regression applications. KNN classifiers take the test instance and map the new instance to the most similar category [21]. Initially, an optimum number of k neighbours are assigned to the algorithm. The algorithm calculates the Euclidean distance of the test instance to elect the k neighbours and those with minimum distances are taken as the neighbours. From each of the elected neighbours, the data point count from each category is evaluated. The new test instance is assigned to the neighbour with the maximum data point count. The model is trained for three target classes namely Regular, Pneumonia and COVID-19.

3. Results and Discussions

This section discusses the results obtained in POCUS data set using the proposed pipeline. We evaluated Accuracy, F1-Score, Precision, Specificity, Sensitivity and Area Under Curve(AUC) metrics and compared them with other state-of-the-art-techniques that use ultrasound images for disease prediction. The whole study is carried out on Intel core i5 processor with 8GB RAM and a GPU support of 4GB.

3.1. Parameter Setting

The various parameters used in the proposed method are set empirically. The parameter setting for MRFO and KNN used in the proposed model is mentioned in the Table 1. The k value denotes the number of neighbours assigned for prediction by KNN. The optimum *k* value is obtained using the trial-and-error method. LL and UL denote the lower limit and the upper limit used in MRFO algorithm.

Table 1. Parameter setting for MRFO & KNN

Parameters	Value
Number of iterations	100
Number of Solutions	10
LL,UL	0,1
Somersault Factor	2
Threshold	0.5
k	5

3.2. Classification Results

The proposed framework was built with a pre-trained network held as the backbone of the model. Experimental analysis was performed using various pre-trained networks for evaluation. Model evaluation is conducted using the POCUS dataset of which 70% of the data has been used for training and the remaining data serves as the test dataset. The effectiveness of the proposed system is tested using various pre-trained models as given in Table 2.

Analysis has been performed using InceptionResnetV2 [22], EfficientnetB0 [23], Xception [24], Darknet-53 [25], Resnet101 [26], VGG-19 [27], Densenet201 [28],Googlenet [29], Shufflenet [30], Squeezenet [31], InceptionV3 [32] and MobilenetV2 [33]. Among the various models tested, the performance of MobilenetV2 is slightly better than the remaining pre-trained networks.

MobilenetV2 obtained the highest overall accuracy of 99.4337%. Figure 3 represents the confusion matrix of MobilenetV2. Using MobilenetV2 as the backbone, 289 images among the 290 COVID-19 LUS images in the test data were correctly classified. The model has achieved a per class Positive Prediction Value (PPV) of 1, 0.98 and 1 for COVID-19, Pneumonia and healthy classes, respectively. An overall PPV of 99.3333% is achieved by the network. The overall recall and F1-score rate of the model are 99.6666% and 99.3333%, respectively. Figure 6 depicts the convergence plot of the network obtained while passing the feature set to the MRFO evolutionary algorithm. A stable fitness solution is obtained near to 50th iteration.

Pre-trained model	Recall	F1-Score	PPV	Accuracy
MobilenetV2	99.6666	99.3333	99.3333	99.4337
Resnet101	99.6666	99.3333	99.3333	99.3205
Shufflenet	99.3333	99.0000	99.0000	99.2072
Densenet201	99.3333	99.3333	99.0000	99.2072
EfficientnetB0	99.3333	99.0000	98.6666	99.0940
InceptionV3	99.3333	99.0000	99.0000	98.9807
Xception	99.0000	98.6666	98.3333	98.8675
InceptionResnetV2	98.6666	97.6666	98.6666	98.1880
VGG19	98.6666	98.6666	98.3333	98.7542
Googlenet	98.6666	98.6666	98.3333	98.7542
Darknet-53	99.0000	98.6666	98.6666	98.7542
Squeezenet	97.6666	97.6666	97.6666	98.0747

Table 2. Performance of various CNNs using MRFO and KNN

Fig. 3: Confusion Matrix obtained with MobilenetV2

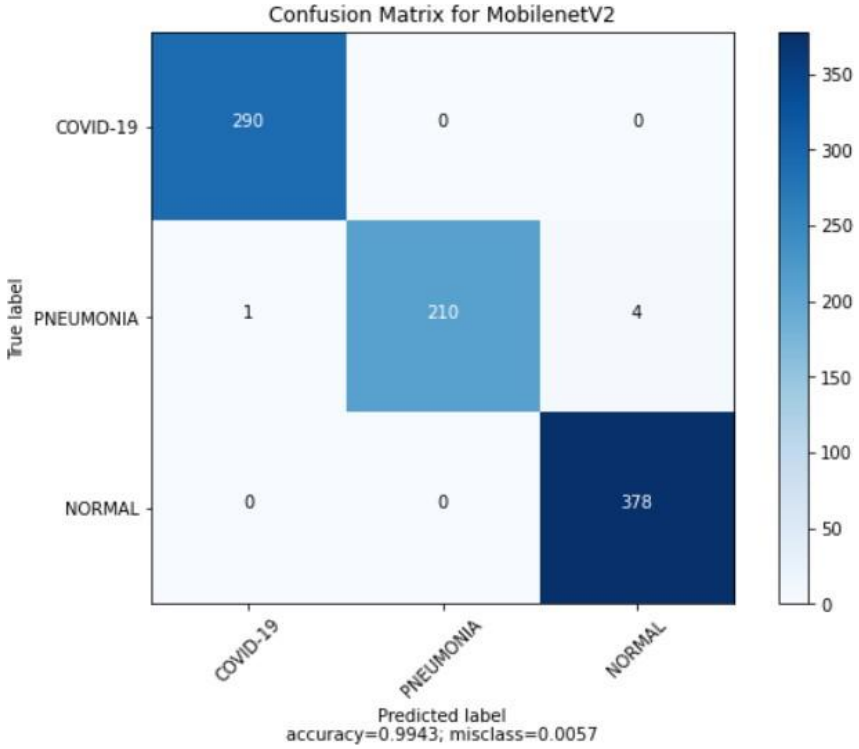

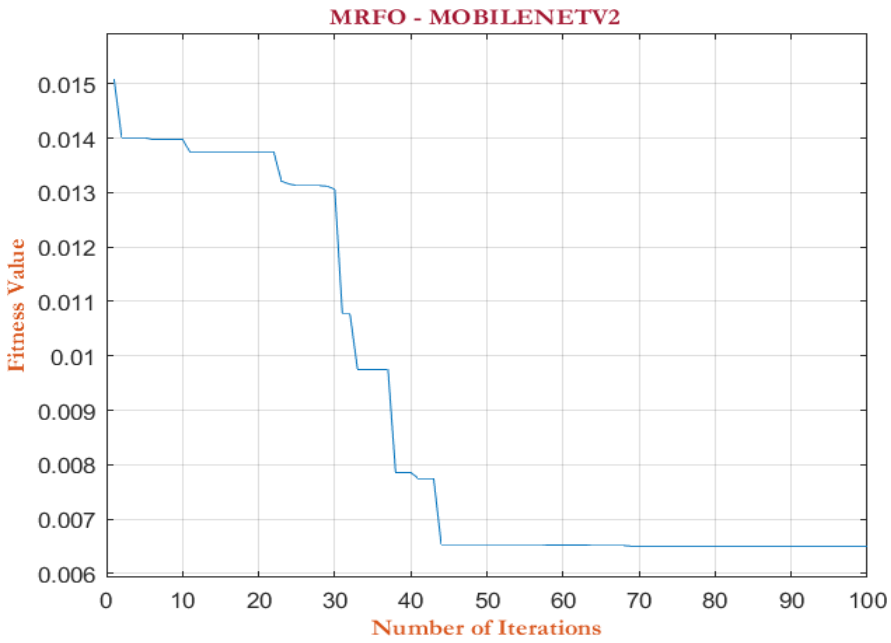

Fig.4. Convergence Plot of MRFO using MobilenetV2

3.3. Statistical analyzes of MRFO with other nature optimisation techniques

The model performance has been statistically analyzed using various feature selection techniques. The choice of MRFO accounts for the fact that it outperforms other optimization techniques in terms of detection accuracy. For the selection of feature optimization techniques, experimental analysis was conducted using both filter and nature inspired optimization techniques. The nature inspired techniques namely, Butterfly Optimization Algorithm (BOA) [34] and Simulated Annealing (SA) [35], and filter selection techniques such as Relieff [36], Pearson Correlation Coefficient (PCC) [37], Neighbourhood Component Analysis (NCA) [38] and Term Variance feature selection techniques were adopted for comparison with the proposed model. The features were extracted using MobilenetV2 and then passed to these optimization techniques for feature selection. The selected features were passed into KNN classifier for model evaluation. Table 3 depicts the performance comparison of MRFO with other feature optimisation techniques

3.4. Statistical analysis of KNN with other classifiers

The experimental evaluation of the model with various classifiers has been conducted using WEKA tool [39][40], an open-source tool for data mining analysis. The analysis had proven the model's efficiency while using KNN as off-the-shelf classifier. For performance analysis, features were extracted from light-weight MobilenetV2 architecture and passed to different classifiers. For performance analysis Bayesnet, SVM, Random Forest, Adaboost, Naive Bayes and Multi-Layer Perceptron (MLP) were considered. The lowest performance has been exhibited by Adaboost with a classification accuracy of 54.1336%. Even though, Random Forest and MLP achieved good results, their performance was significantly lower than that of KNN. Table 4 depicts the performance analysis of the model with different classifiers.

3.5. Statistical analyzes of the proposed model with other state of art methods.

Very few research works in literature have utilized lung ultrasound images for the diagnosis of COVID-19. Table 5 shows the comparison of results with recent techniques employing ultrasound images for disease prediction. A quantitative analysis is not possible as each of the reported works use different amount of data for result analysis. Hence, a qualitative comparison is performed with these state-of-art research works. It is worth to note that our proposed model outperforms all other techniques and performed well in disease prediction. Table 5 shows performance comparison of the proposed model with other state-of-the-art methods.

4. Conclusion

The COVID-19 pandemic is spreading across the world very rapidly. Due to the increasing cases of victims, manual diagnosis of the disease has become a tedious task to the medical professionals. Therefore, fast and accurate diagnosis of the disease is beneficial for the control of the virus.

This work concentrates on the computer-aided diagnosis of COVID-19 using lung ultrasound images of the victims.

The high sensitivity obtained shows the efficacy of the proposed technique in distinguishing COVID-19, Pneumonia and healthy classes using the images from the ultrasound scan. The experimental analysis illustrates the effectiveness of pre-trained CNN in combination with nature inspired algorithm and KNN for the diagnosis of COVID-19 in lung ultrasound images. The model can be extended to detect the severity of the infection in the near future.

Table 3. Performance comparison of feature selection techniques

Pre-trained model	Selection Method	Sensitivity	F1-Score	Precision	Accuracy
MobilenetV2	Proposed	99.6666	99.3333	99.3333	99.4337
MobilenetV2	BOA	99.0000	98.6666	98.6666	98.9807
MobilenetV2	SA	99.0000	98.6666	98.6666	98.9807
MobilenetV2	Relieff	98.3333	98.0000	97.6666	98.0747
MobilenetV2	TV	98.6666	98.3333	97.6666	98.4145
MobilenetV2	PCC	98.3333	98.0000	97.6666	98.0747

Table 4. Performance comparison of the proposed classifier with other classifiers integrated with MRFO.

Pre-trained model	Classifier	Sensitivity	F1-Score	Precision	Accuracy
MobilenetV2	Proposed	99.6666	99.3333	99.3333	99.4337
MobilenetV2	Bayesnet	81.1000	81.2000	81.7000	81.0875
MobilenetV2	SVM	91.5000	91.5000	91.6000	91.5062
MobilenetV2	Random Forest	95.4000	95.3000	95.4000	95.3567
MobilenetV2	Adaboost	54.1000	48.0000	50.4000	54.1336
MobilenetV2	Naive Bayes	80.6000	80.7000	80.9000	80.6342
MobilenetV2	MLP	96.0000	96.0000	96.1000	96.0362

Table 5. Model performance comparison with other state-of-the-art methods.

Method	Number of images	Sensitivity	F1-Score	Precision	Accuracy
Proposed	969 COVID-19 vs 714 pneumonia vs 1261 Regular	99.3000	99.6000	99.0000	99.4300
Born et al. [4]	1204 COVID-19 vs 704 pneumonia vs 1326 Regular	96.0000	-	-	89.0000
Hossain et al. [16]	(Videos)45 COVID-19 vs 23 Pneumonia vs 53 Regular	93.2000	-	-	92.5000
Aswathi et al. [17]	678 COVID-19 vs 277 Pneumonia vs 182 Regular	-	-	-	83.2000
Born et al. [41]	693 COVID-19 vs 377 Pneumonia vs 295 Regula	-	-	-	90.0000

References

[1] ZIKA. Novel coronavirus (2019-ncov). 2020.

[2] Didier Raoult, Alimuddin Zumla, Franco Locatelli, Giuseppe Ippolito, and Guido Kroemer. Coronavirus infections: Epidemiological, clinical and immunological features and hypotheses. Cell stress, 4(4):66, 2020.

[3] World Health Organization et al. Coronavirus disease (covid-19): similarities and differences with influenza. Accessed September, 7, 2020.

[4] Jannis Born, Gabriel Bra¨ndle, Manuel Cossio, Marion Disdier, Julie Goulet, Je´re´mie Roulin, and Nina Wiedemann. Pocovid-net: automatic detection of covid-19 from a new lung ultrasound imaging dataset (pocus). arXiv preprint arXiv:2004.12084, 2020.

[5] Jannis Born, Nina Wiedemann, Manuel Cossio, Charlotte Buhre, Gabriel Bra¨ndle, Konstantin Leidermann, Avinash Aujayeb,

Michael Moor, Bastian Rieck, and Karsten Borgwardt. Accelerating detection of lung pathologies with explainable ultrasound image analysis. Applied Sciences, 11(2):672, Jan 2021. ISSN 2076-3417. doi: 10.3390/app11020672. URL: http://dx.doi.org/10.3390/app11020672.

[6] J Born, N , Wiedemann, M Cossio, C Buhre, G Bra¨ndle, K

Leidermann, and A Aujayeb. L2 accelerating covid-19 differential diagnosis with explainable ultrasound image analysis: an ai tool. Thorax, 76(Suppl 1):A230–A231, 2021. ISSN 0040-6376. doi: 10.1136/thorax-2020-BTSabstracts.404. URL https: /thorax.bmj.com/content/76/Suppl_1/A230.2.

[7] World Health Organization et al. The effects of virus variants on covid-19 vaccines, 2021.

[8] Liqa A Rousan, Eyhab Elobeid, Musaab Karrar, and Yousef Khader. Chest x-ray findings and temporal lung changes in patients with covid-19 pneumonia. BMC Pulmonary Medicine, 20(1):1–9, 2020.

[9] Thomas C Kwee and Robert M Kwee. Chest ct in covid-19: what the radiologist needs to know. RadioGraphics, 40(7):1848–1865, 2020.

[10] Yao Zhang, Heng Xue, Mixue Wang, Nan He, Zhibin Lv, and Ligang Cui. Lung ultrasound findings in patients with coronavirus disease (covid-19). American Journal of Roentgenology, 216(1):80–84, 2021.

[11] Bejoy Abraham and Madhu S Nair. Computer-aided detection of covid-19 from ct scans using an ensemble of cnns and ksvm classifier. Signal, Image and Video Processing, pages 1–8, 2021.

[12] JL Gayathri, Bejoy Abraham, MS Sujarani, and Madhu S Nair. A computer-aided diagnosis system for the classification of covid-19 and non-covid-19 pneumonia on chest x-ray images by integrating cnn with sparse autoencoder and feed forward neural network. Computers in Biology and Medicine, 141:105134, 2022.

[13] Nagur Shareef Shaik and Teja Krishna Cherukuri. Transfer learning based novel ensemble classifier for covid-19 detection from chest ct-scans. Computers in Biology and Medicine, 141:105127, 2022.

[14] Mahesh Gour and Sweta Jain. Uncertainty-aware convolutional neural network for covid-19 x-ray images classification. Computers in biology and medicine, 140:105047, 2022.

[15] Aayush Kumar, Ayush R Tripathi, Suresh Chandra Satapathy, and Yu-Dong Zhang. Sars-net: Covid-19 detection from chest x-rays by combining graph convolutional network and convolutional neural network. Pattern Recognition, 122: 108255, 2022.

[16] Ghulam Muhammad and M Shamim Hossain. Covid-19 and non-covid-19 clas- sification using multi-layers fusion from lung ultrasound images. *Information Fusion*, 72:80–88, 2021.

[17] Navchetan Awasthi, Aveen Dayal, Linga Reddy Cenkeramaddi, and Phaneendra K Yalavarthy. Mini-covidnet: Efficient lightweight deep neural network for ultrasound based point-of-care detection of covid-19. *IEEE Transactions on Ul- trasonics, Ferroelectrics, and Frequency Control*, 68(6):2023–2037, 2021.

[18] Shai Bagon. A framework for integrating domain knowledge into deep networksfor lung ultrasound, and its applications to covid-19. 2021.

[19] Jia Deng, Wei Dong, Richard Socher, Li-Jia Li, Kai Li, and Li Fei-Fei. Imagenet: A large-scale hierarchical image database. In *2009 IEEE conference on computervision and pattern recognition*, pages 248–255. Ieee, 2009.

[20] Weiguo Zhao, Zhenxing Zhang, and Liying Wang. Manta ray foraging optimiza- tion: An effective bio-inspired optimizer for engineering applications. *Engineering Applications of Artificial Intelligence*, 87:103300, 2020.

[21] Kashvi Taunk, Sanjukta De, Srishti Verma, and Aleena Swetapadma. A brief review of nearest neighbor algorithm for learning and classification. In *2019 International Conference on Intelligent Computing and Control Systems (ICCS)*,pages 1255–1260. IEEE, 2019.

[22] Christian, Sergey Ioffe, Szegedy, Vincent Vanhoucke, and Alex Alemi. Inception-v4, inception-resnet and the impact of residual connections on learning. *arXiv preprint arXiv:1602.07261*, 2016.

[23] Mingxing Tan and Quoc V Le. Efficientnet: Rethinking

model scaling for convolutional neural networks. *arXiv preprint arXiv:1905.11946*, 2019.

[24] François Chollet. Xception: Deep learning with depthwise separable convolutions. In *Proceedings of the IEEE conference on Computer Vision and Pattern Recognition*, pages 1251–1258, 2017.

[25] Joseph Redmon and Ali Farhadi. Yolov3: An incremental improvement. *arXiv preprint arXiv:1804.02767*, 2018.

[26] Zifeng Wu, Chunhua Shen, and Anton Van Den Hengel. Wider or deeper: Revisiting the resnet model for visual recognition. *Pattern Recognition*, 90:119–133, 2019.

[27] Karen Simonyan and Andrew Zisserman. Very deep convolutional networks forlarge-scale image recognition. *arXiv preprint arXiv:1409.1556*, 2014.

[28] Gao Huang, Zhuang Liu, Laurens Van Der Maaten, and Kilian Q Weinberger. Densely connected convolutional networks. In *Proceedings of the IEEE conference on computer vision and pattern recognition*, pages 4700–4708, 2017.

[29] Christian Szegedy, Wei Liu, Yangqing Jia, Pierre Sermanet, Scott Reed, Dragomir Anguelov, Dumitru Erhan, Vincent Vanhoucke, and Andrew Rabinovich. Goingdeeper with convolutions. In *Proceedings of the IEEE conference on computer vision and pattern recognition*, pages 1–9, 2015

[30] Xiangyu Zhang, Xinyu Zhou, Mengxiao Lin, and Jian Sun. Shufflenet: An ex- tremely efficient convolutional neural network for mobile devices. In *Proceedingsof the IEEE conference on computer vision and pattern recognition*, 2018.

[31] Forrest N Iandola, Song Han, Matthew W Moskewicz, Khalid Ashraf, William J Dally, and Kurt Keutzer. Squeezenet: Alexnet-level accuracy with 50x fewer parameters and¡ 0.5 mb model size. *arXiv preprint arXiv:1602.07360*, 2016.

[32] Christian Szegedy, Vincent Vanhoucke, Sergey Ioffe, Jon Shlens, and Zbigniew Wojna. Rethinking the inception architecture for computer vision. In *Proceedings of the IEEE conference on Computer Vision and Pattern Recognition*, pages2818–2826, 2016.

[33] Mark Sandler, Andrew Howard, Menglong Zhu, Andrey Zhmoginov, and Liang- Chieh Chen. Mobilenetv2: Inverted residuals and linear bottlenecks. In *Proceed-ings of the IEEE conference on Computer Vision and Pattern Recognition*, pages4510–4520, 2018.

[34] Sankalap Arora and Satvir Singh. Butterfly optimization algorithm: a novel approach for global optimization. *Soft Computing*, 23(3):715–734, 2019.

[35] Peter JM Van Laarhoven and Emile HL Aarts. Simulated annealing. In *Simulated annealing: Theory and applications*, pages 7–15. Springer, 1987.

[36] Newton Spolaôr, Everton Alvares Cherman, Maria Carolina Monard, and Huei Diana Lee. Relieff for multi-label feature selection. In *2013 Brazilian Conference on Intelligent Systems*, pages 6–11. IEEE, 2013.

[37] Jacob Benesty, Jingdong Chen, Yiteng Huang, and Israel Cohen. Pearson correlation coefficient. In *Noise reduction in speech processing*, pages 1–4. Springer, 2009.

[38] Wei Yang, Kuanquan Wang, and Wangmeng Zuo. Neighborhood component feature selection for high-dimensional data. *J. Comput.*, 7(1):161–168, 2012.

[39] Ian H Witten, Eibe Frank, Mark A Hall, CJ Pal, and MINING DATA. Practical machine learning tools and techniques. In *DATA MINING*, volume 2, page 4, 2005.

[40] Mark Hall, Eibe Frank, Geoffrey Holmes, Bernhard Pfahringer, Peter Reutemann,and Ian H Witten. The weka data mining software: an update. *ACM SIGKDD explorations newsletter*, 11(1):10–18, 2009.

[41] Jannis Born, Nina Wiedemann, Gabriel Brändle, Charlotte Buhre, Bastian Rieck, and Karsten Borgwardt. Accelerating covid-19 differential diagnosis with explainable ultrasound image analysis. *arXiv preprint arXiv:2009.06116*, 2020.